

Article

Mesomorphic Behaviour and DFT Insight of Arylidene Schiff Base Liquid Crystals and Their Pyridine Impact Investigation

Mohamed A. Zakaria ¹, Mohammed Alazmi ¹, Kanubhai D. Katariya ², Yeldezh El Kilany ¹, El Sayed H. El Ashry ¹, Mariusz Jaremko ³, Mohamed Hagar ^{1,4,*} and Sayed Z. Mohammady ⁵

¹ Department of Chemistry, Faculty of Science, Alexandria University, Alexandria 21321, Egypt; mohamed.zakaria@alexu.edu.eg (M.A.Z.); Mohammadalazmmi@gmail.com (M.A.); yeldezh244@yahoo.com (Y.E.K.); eelashry60@hotmail.com (E.S.H.E.A.)

² Department of Chemistry, Faculty of Science, the Maharaja Sayajirao University of Baroda, Vadodara-390002, Gujarat, India; kanukatariya-chemphd@msubaroda.ac.in

³ Biological and Environmental Sciences & Engineering Division (BESE), King Abdullah University of Science and Technology (KAUST), Thuwal 23955-6900, Saudi Arabia; mariusz.jaremko@kaust.edu.sa

⁴ Department of Chemistry, College of Sciences, Taibah University, Yanbu 46423, Saudi Arabia

⁵ Department of Chemistry, College of Science, King Saud University, Riyadh 11451, Saudi Arabia; sahmed2.c@ksu.edu.sa

* Correspondence: mohamedhagar@gmail.com

Abstract: A new series of Schiff base liquid crystal have been prepared and studied. Schiff bases of p-alkyl aniline derivatives and 4-phenyl pyridine-4'-carbaldehyde were prepared. The terminal alkyl groups substituting aniline are of varied chain length, namely C8, C12 and C14. The structures of the compounds were elucidated by ¹H NMR and ¹³C NMR. The mesomorphic thermal and optical characteristics of the samples were determined via differential thermal analysis (DSC) and polarization optical microscopy (POM). All compounds exhibit enantiotropic dimorphic mesophase behaviour, referred to as smectic X1 (SmX1) and smectic X2 (Sm A). Experimental results obtained for the mesophases were correlated with density functional theory (DFT) theoretical calculations. The results of the new series are further compared to two series of compounds bearing pyridine (two ring Schiff bases) and biphenyl, respectively, in their mesogens. The series of compounds of one pyridine ring are generally not mesomorphic. The results indicate that the alkyl chain length has a strong impact on the mesomorphic characteristics and thermal stabilities of the different mesophases. As a trend, the temperature ranges of both of smectic mesophases of all compounds are higher in new compounds bearing the 4-phenyl pyridine moiety. In addition, the total mesophase range is generally higher in the new compounds when compared to their biphenyl analogues. Finally, theoretical DFT calculations were performed to illustrate the experimental finding of the mesomorphic behaviour in terms of the molecular geometry and aromaticity, π - π stacking and LOL- π .

Keywords: liquid crystal; schiff base; biphenyl; 4-phenyl pyridine; DFT



Citation: Zakaria, M.A.; Alazmi, M.; Katariya, K.D.; El Kilany, Y.; El Ashry, E.S.H.; Jaremko, M.; Hagar, M.; Mohammady, S.Z. Mesomorphic Behaviour and DFT Insight of Arylidene Schiff Base Liquid Crystals and Their Pyridine Impact Investigation. *Crystals* **2021**, *11*, 978. <https://doi.org/10.3390/cryst11080978>

Academic Editor: Antonio Martins Figueiredo Neto

Received: 9 July 2021

Accepted: 14 August 2021

Published: 18 August 2021

Publisher's Note: MDPI stays neutral with regard to jurisdictional claims in published maps and institutional affiliations.



Copyright: © 2021 by the authors. Licensee MDPI, Basel, Switzerland. This article is an open access article distributed under the terms and conditions of the Creative Commons Attribution (CC BY) license (<https://creativecommons.org/licenses/by/4.0/>).

1. Introduction

Liquid crystals (LCs) are an attractive class of soft matter with properties that fall somewhere between liquids and solid crystals [1–3]. They have gained a huge amount of attention due to their very promising applications in various technological fields such as organic field effect transistors (OFETs) [4], Pancharatnam-Berry (PB) microlense [5], liquid crystal elastomers [6], sunlight-driven polymer actuators [7], photovoltaics [8], biosensors [9–11] and telecommunications [12]. The design and development of new low cost liquid crystalline materials with a long mesophase temperature range and high thermal stability will always be a challenge, especially for thermotropic LCs, due to their extensive and potential applications in various fields. An effective way to develop new low cost LC material with unique properties is the chemical modification of geometry which has proven to be one of the finest strategies.

In particular, in calamitic liquid crystals (rod like), the mesomorphic behaviour can be significantly altered by even a minor change in the molecular geometry including various connecting units, variation in terminal chains (size and type), the inclusion of heteroatoms/heterocyclic ring and the existence of various laterally substituted atoms/groups [13]. Consequently, several types and classes of substituents with different polarity have been repeatedly amalgamated into diverse LC structures to alter the conformational and geometrical preferences, the mesomorphic properties, the transition temperature and some additional crucial physical properties not just important for designing and developing new low cost LC materials with enhanced properties appropriate for display technologies, but also for recognizing the structure–property relationship.

Schiff bases represent a substantial class of organic compounds embracing imine (-C=N-) linkage. Schiff bases are involved in many appealing applications in diverse fields including catalysis [14], medicine [15], corrosion chemistry [16] and photochromism [17]. They have been extensively studied for their interesting liquid crystalline properties [18–24] as they provide rigid core structure and enhance mesophase formation by preserving a linear geometry, higher stability and polarity of imine linkage [25].

Since the discovery of LCs, the compounds possessing heteroatoms (N, O, S) or heterocyclic rings as a part of their molecular structures have been widely studied. Incorporation of heteroatoms/heterocyclic rings into rod-like LC molecules largely affects the molecular geometry, mesomorphic characteristics, phase transitions, thermal stability and dielectric properties as a result of the polarizability of heteroatoms leading to production of advanced functional materials with fascinating mesomorphic properties. A number of mesogenic compounds possessing heterocyclic units such as pyridine [26], thiophene [27] and 1,3,4-thiadiazole [28], oxadiazole [29] and oxazole [30] in the rigid core in many LCs have been widely studied.

The rod-like LCs involving pyridine (a simplest six membered heterocyclic aromatic ring) participating in the core rigid unit exhibited exciting mesomorphic properties that have been extensively studied for designing new LC molecules [13,31–33]. The place at which the nitrogen atom is located in the pyridine unit and its position in the core rigid structure of LC molecules significantly affect the mesomorphic properties of pyridine-based compounds [34]. This can be rationalized to the expected influence on the dipole moment, the dielectric nature of the compounds, the dispersion forces and the polarizability of the molecule [35]. In addition, this affects the molecular staking during mesophase and hence displays fascinating mesophase behaviour. The terminal heterocyclic ring has a reasonable impact on the dipole moment. Therefore, the position of the nitrogen atom in the rod-like LC also influences the mesophase stability [36]. In rod-like LCs containing pyridine in their rigid core, compounds possessing pyridine may also serve as charge-transfer donors in binary systems (based on the position of the pyridine ring) [37].

The present work represents a comparative study between three Schiff base LC series bearing in their mesogens the pyridine [38], biphenyl [39] and 4-phenyl pyridine. The thermal and mesomorphic behaviour of the new series containing 4-phenyl pyridine will be studied experimentally by means of differential thermal analysis (DSC) and polarization optical microscopy (POM). These results will be discussed theoretically in the frame of density field theory (DFT).

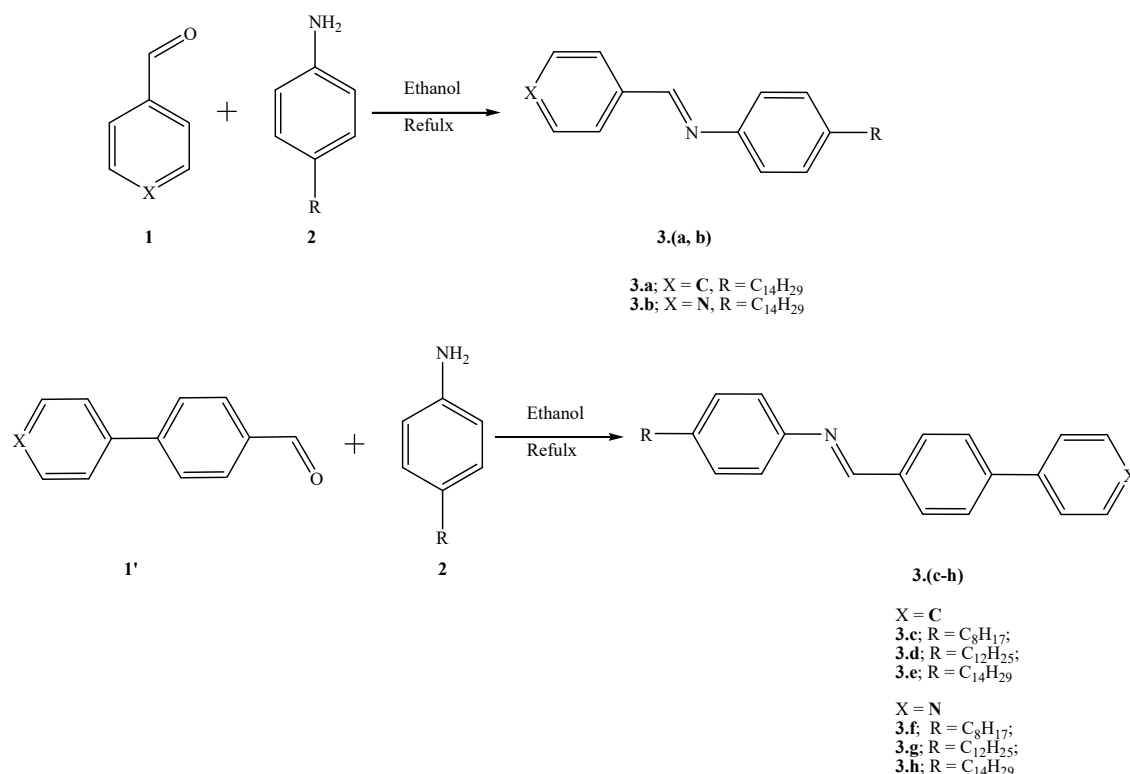
2. Materials and Methods

All chemicals were purchased from TCI Company, Japan. Their purity is higher than 98%. Schiff bases were prepared and recrystallized twice from an ethanol/water mixture and were confirmed to be thin-layer chromatography (TLC) pure, Scheme 1.

2.1. Synthesis of *N*-arylidene-4-alkylbenzenamine (3.a–3.h)

Equimolar equivalents of formyl derivative and 4-arylamine (4.1 mmol) were dissolved in ethanol (10 mL) and refluxed for two hours. The mixture was filtered after cooling

to room temperature. The obtained solid was washed with cold ethanol and recrystallized twice from hot ethanol to yield pure compounds.



Scheme 1. Synthesis of N-arylidene-4-alkylbenzenamine 3.a–3.h.

***N*-(4-(Pyridin-4-yl)benzylidene)-4-octylbenzenamine (3.f)**

Yield = 98%, R_f = 0.6, IR (KBr, cm⁻¹): 3032, 2956, 2849 (C-H), 1623 (CH=N), 1594, 1538, 1502, 1404, 1360, 1273, 1183, 1112, 889, 822, 804, 721; ¹H NMR (400 MHz, CDCl₃, δ ppm): 0.90 (t, J = 6.4 Hz, 3H), 1.29–1.34 (m, 10H), 1.61–1.68 (m, 2H), 2.65 (t, J = 7.6 Hz, 2H), 7.20–7.26 (m, 4H), 7.58 (dd, J = 6.0 Hz, 2H), 7.77 (d, J = 8.4 Hz, 2H), 8.03 (d, J = 8.4 Hz, 2H), 8.55 (s, 1H), 8.71 (dd, J = 6.4 Hz, 2H); ¹³CNMR (100 MHz, CDCl₃, δ ppm): 14.16 (-CH₃), 22.71, 29.31, 29.34, 29.52, 31.59, 31.92, 35.56 (-CH₂), 120.89, 121.60, 127.38, 129.21, 129.41, 136.99, 140.59, 141.39, 147.46, 149.28, 150.43, 158.49 (CH=N). Anal.Calc for C₂₆H₃₀N₂: C, 84.28; H, 8.16; N, 7.56; found: C, 83.97; H, 7.85; N, 7.06%.

***N*-(4-(Pyridin-4-yl)benzylidene)-4-dodecylbenzenamine (3.g)**

Yield = 97%, R_f = 0.6, IR (KBr, cm⁻¹): 2955, 2917, 2848 (C-H), 1622 (CH=N), 1594, 1538, 1502, 1404, 1360, 1230, 1113, 844, 821, 720; ¹H NMR (400 MHz, CDCl₃, δ ppm): 0.90 (t, J = 6.8 Hz, 3H), 1.28 (s(br), 18 H), 1.61–1.68 (m, 2H), 2.65 (t, J = 7.6 Hz, 2H), 7.20–7.26 (m, 4H), 7.58 (dd, J = 6.0 Hz, 2H), 7.77 (d, J = 8.4 Hz, 2H), 8.04 (d, J = 8.4 Hz, 2H), 8.56 (s, 1H), 8.72 (dd, J = 6.0 Hz, 2H); ¹³CNMR (100 MHz, CDCl₃, δ ppm): 14.17 (-CH₃), 22.73, 29.33, 29.39, 29.55, 31.64, 31.67, 29.69, 31.59, 31.95, 35.55 (-CH₂), 120.88, 121.61, 127.38, 129.21, 129.41, 136.99, 140.59, 141.39, 147.47, 149.28, 150.43, 158.49 (CH=N). Anal.Calc. for C₃₀H₃₈N₂: C, 84.46; H, 8.98; N, 6.57; found: C, 84.05; H, 8.58; N, 5.97%.

***N*-(4-(Pyridin-4-yl)benzylidene)-4-tetradecylbenzenamine (3.h)**

Yield = 95%, R_f = 0.5, IR (KBr, cm⁻¹): 2956, 2916, 2849 (C-H), 1623 (CH=N), 1594, 1538, 1502, 1404, 1360, 1202, 1114, 889, 804, 721; ¹H NMR (400 MHz, CDCl₃, δ ppm): 0.90 (t, J = 6.4 Hz, 3H), 1.27–1.33 (m, 22 H), 1.61–1.68 (m, 2H), 2.65 (t, J = 7.6 Hz, 2H), 7.20–7.26 (m, 4H), 7.58 (dd, J = 6.0 Hz, 2H), 7.77 (d, J = 8.4 Hz, 2H), 8.04 (d, J = 8.4 Hz, 2H), 8.56 (s, 1H), 8.72 (dd, J = 6.4 Hz, 2H); ¹³CNMR (100 MHz, CDCl₃, δ ppm): 14.17 (-CH₃), 22.72, 29.33, 29.39, 29.55, 29.63, 29.69, 29.71, 31.59, 31.95, 35.55 (-CH₂), 120.88, 121.61, 127.38, 129.21,

129.41, 136.99, 140.60, 141.40, 147.47, 149.28, 150.43, 158.49 (CH=N). C₃₂H₄₂N₂ Anal.Calc. for C₃₂H₄₂N₂; C, 84.53; H, 9.31; N, 6.16; found: C, 84.42; H, 9.05; N, 5.86%.

The phase changes in the materials were determined via differential scanning calorimetry (DSC), DSC-60A, Shimadzu, Japan. Specimens of the size 2–3 mg were encapsulated in aluminum pans and were heated or cooled under a dry nitrogen atmosphere. Measurements were performed at 10.0 °C/min. Samples were heated from room temperature to 200 °C and cooled back to room temperature at the same heating rate, all under an inert nitrogen gas atmosphere. The phase transition temperature values were determined from the endothermic peak minima of enthalpy in the heating curves. The accuracy of temperature monitoring was better than 1.0 °C.

Transition temperatures for the prepared compounds were checked and phases were identified by polarized optical microscope (POM, Wild, Germany) attached with Mettler FP82HT hot stage.

2.2. Computational Method

Gaussian 09 software was used for DFT calculations for the studied compounds [24]. DFT/B3LYP methods using a 6-31G (d,p) basis set was selected for the calculations. The geometries were optimized by minimizing the energies with respect to all geometrical parameters without imposing any molecular symmetry constraints. The structures of the optimized geometries were drawn with Gauss View [25]. Moreover, calculation of frequencies was carried out by the same level of theory. The frequency calculations showed that all structures were stationary points in the geometry optimization method with no imaginary frequencies.

3. Results and Discussion

3.1. Synthesis and Characterization

In the FT-IR spectra of compounds, the absorption bands at 2955, 2917 and 2848 cm⁻¹ correspond to the aliphatic methyl and methylene groups. The absorption band at 1623 cm⁻¹ corresponds to the imine (CH=N) Schiff base conjugated with an aromatic ring. Overall, the results of FT-IR analysis revealed that the position of absorption bands was not affected by the variation of length of the alkoxy chain.

In the ¹H NMR of compounds **3.f** and **3.g**, the terminal –CH₃ protons were observed at δ 0.90 ppm as a triplet, whereas the methylene protons directly attached to the aromatic ring appeared as a triplet at δ 2.65 ppm. The proton of imine linkage (–CH=N–) was observed at δ 5.88 ppm as a singlet confirming the existence of a Schiff base for the prepared compounds. The two pyridine protons at ortho position to nitrogen were observed most upfield at δ 8.72 ppm as a doublet. The rest of the aromatic and aliphatic protons were observed as per the substitution pattern of compounds. The ¹³C NMR spectra of compounds **3.f–3.h** showed characteristic signals of carbons. The terminal methyl carbon was observed most downfield at δ 14.16 ppm, while methylene carbon directly attached to the aromatic ring was observed at δ 35.56 ppm. The two carbons in vicinity to the pyridine nitrogen were observed at δ 150.43 ppm and the imine linkage carbon appeared most upfield at δ 158.49s ppm (see Supplementary Materials).

3.2. Mesomorphic Behaviour

Transition temperatures and the corresponding associated enthalpy changes of the prepared compounds **3.b–3.h** were measured by DSC and presented in Table 1. DSC curves of heating/cooling cycles for the new compounds **3.f**, **3.g** and **3.h** are presented in Figure 1. All the newly and previously reported prepared biphenyl [39] and 4-phenyl pyridine compounds displayed dimorphic enantiotropic mesomorphic properties, whereby the corresponding endotherms were regarded as follows according to the increase in temperature: Crystalline to smectic X1 (Cryst.-SmX1), SmX1 to smectic A (SmX1-SmA) and SmA-isotropic (SmA-I) transitions. The SmX1 and SmA mesophases were identified by the presence of the standard Schlieren and focal-conic fan textures.

Table 1. Phase transitions: Temperatures (T , °C), enthalpies (ΔH , kJ/mol) and mesomorphic range (ΔT) for the prepared compounds **3.b–3.h**. SmX1 was identified by the authors in [40] as SmB for samples **3.c**, **3.d** and **3.e**.

Compound	°C T_{Cr-I}	kJ/mol ΔH_{Cr-I}	°C $T_{Cr-SmX1}$	kJ/mol $\Delta H_{Cr-SmX1}$	°C $T_{SmX1-SmA}$	kJ/mol $\Delta H_{SmA-SmX1}$	°C T_{SmA-I}	kJ/mol ΔH_{SmA-I}	°C T_{SmA-N}	kJ/mol ΔH_{SmA-N}	°C T_{N-I}	kJ/mol ΔH_{N-I}
3.b [40]	63.4	11.54										
3.c [39]			95.1	28.09	130.0	3.03			132.2	1.77	134.5	0.46
3.d [39]			105.4	53.10	121.5	5.09	128.6	5.68				
3.e [39]			109.0	46.62	116.9	3.78	124.6	3.71				
3.f			93.9	26.78	102.0	4.16	134.0	3.62				
3.g			105.8	38.23	126.0	3.07	150.1	6.95				
3.h			109.9	40.62	122.1	4.05	130.0	6.52				

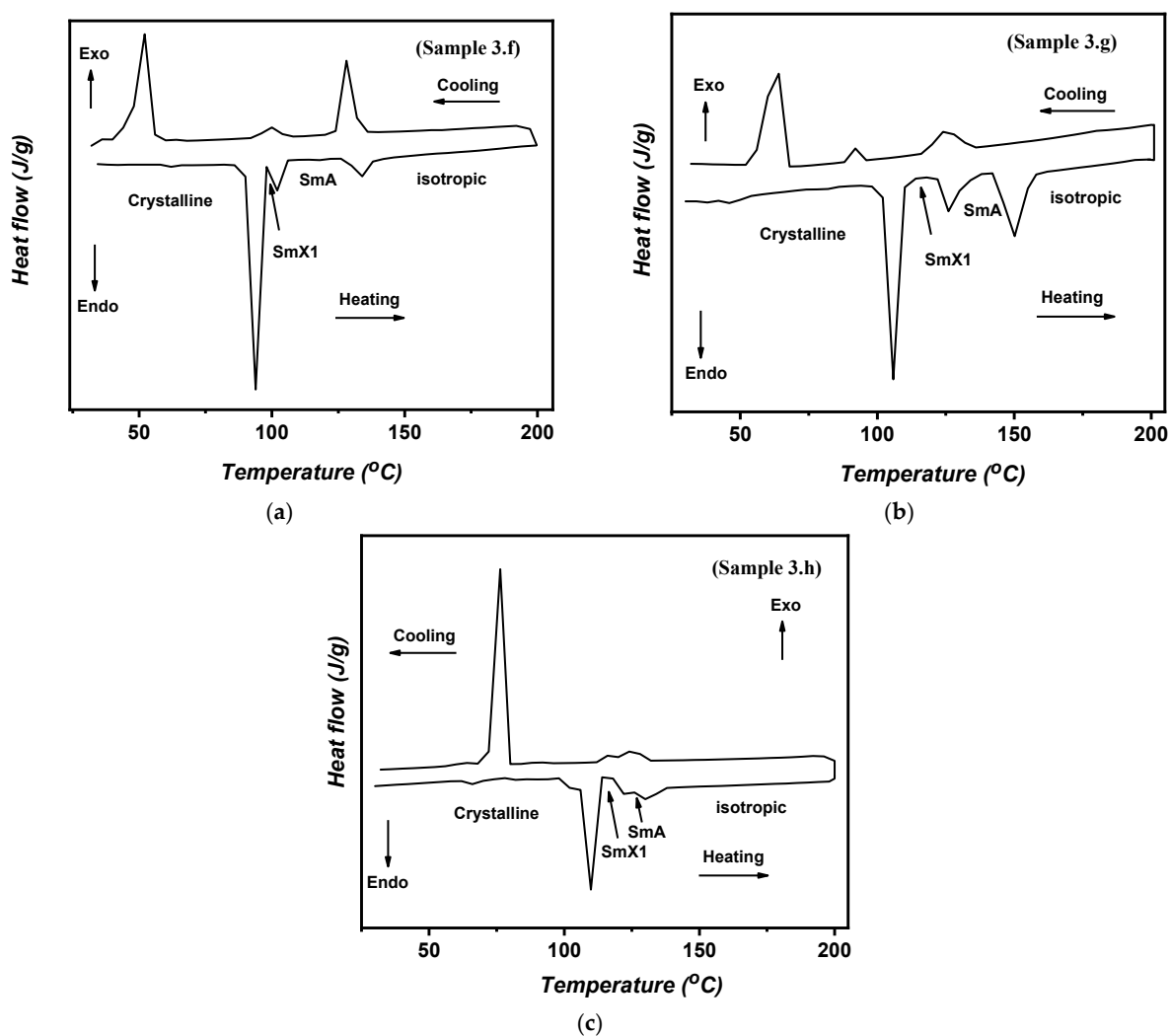


Figure 1. DSC thermograms of compounds **3.f** (a), **3.g** (b) and **3.h** (c) during first heating and cooling cycles (10 °C min^{-1}).

The mesophases of new compounds were recognised by observing their textures through POM (Figure 2). Observation of mesomorphic behaviour of the new compounds bearing the 4-phenylpyridyl mesogens (**3.f** and **3.g**) under the POM revealed enantiotropic dimorphic mesomorphism. Upon heating from crystalline phase to isotropic liquid and again cooling it from its isotropic liquid phase to crystalline phase, all new compounds exhibited the occurrence of two mesophases. The determined ΔH values associated with the two mesophase transitions above the crystalline mesomorphic transition in all samples lie in the range of from 3.07 to 6.95 kJ/mol, assuming the existence of smectic rather than nematic mesophases and this was confirmed by the polarized optical microscopy results,

see Figure 2. In addition, these smectic mesophases were identified via POM by displaying the standard Schlieren and focal-conic fan textures. Unfortunately, we were not able to identify the exact type of the first appearing mesophase by means of POM. Therefore, the two smectic mesophases are distinguished as SmX1 and SmA through all this work, according to their appearance upon heating.

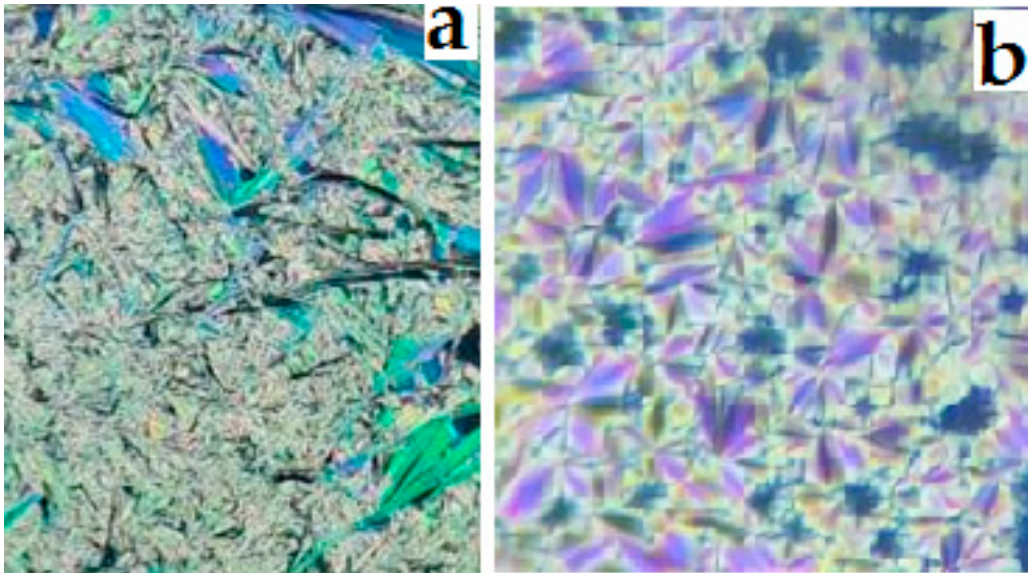


Figure 2. Mesophase textures observed by POM during heating cycle of compound 3.h; (a) SmX1 phase; (b) SmA phase.

The effects of increase in alkyl chain length on the thermal properties of both biphenyl and phenyl pyridine mesogens on the temperature range of the different smectic mesophases as well as the total mesomorphic range of temperature is presented in Figure 3a–c. The results showed an increment in the Cryst.-SmX1 transition temperatures upon the increase of the terminal alkyl group (C8 to C14). It was also observed that the transition temperatures for SmX1-Sm A mesophase change increase as we go from 3.f to 3.g and then decrease for sample 3.h. In addition, the SmA-I transition temperatures revealed a similar response towards the increase of the terminal alkyl group (C8 to C14). Again, the transition temperatures for SmA-I mesophase change increase as we go from 3.f to 3.g and then decrease for sample 3.h.

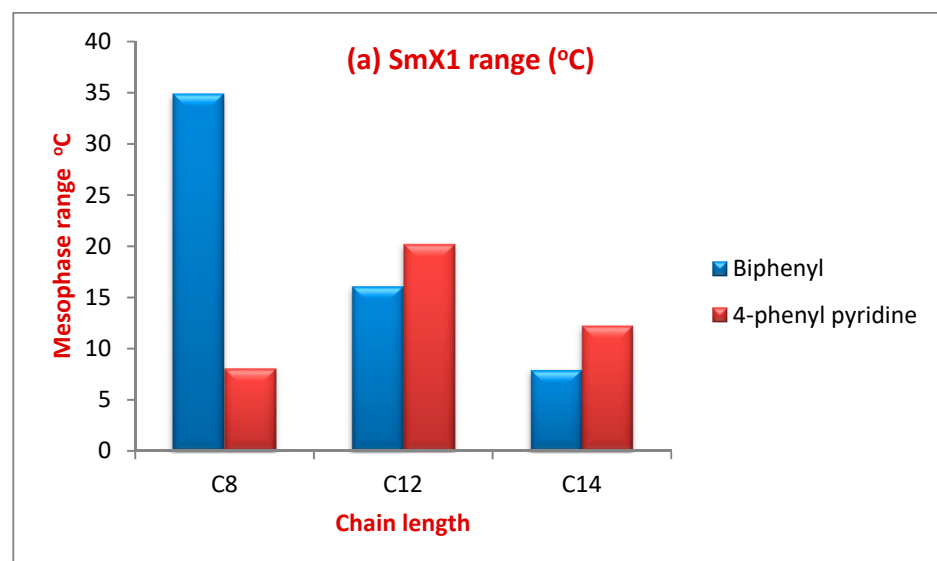


Figure 3. Cont.

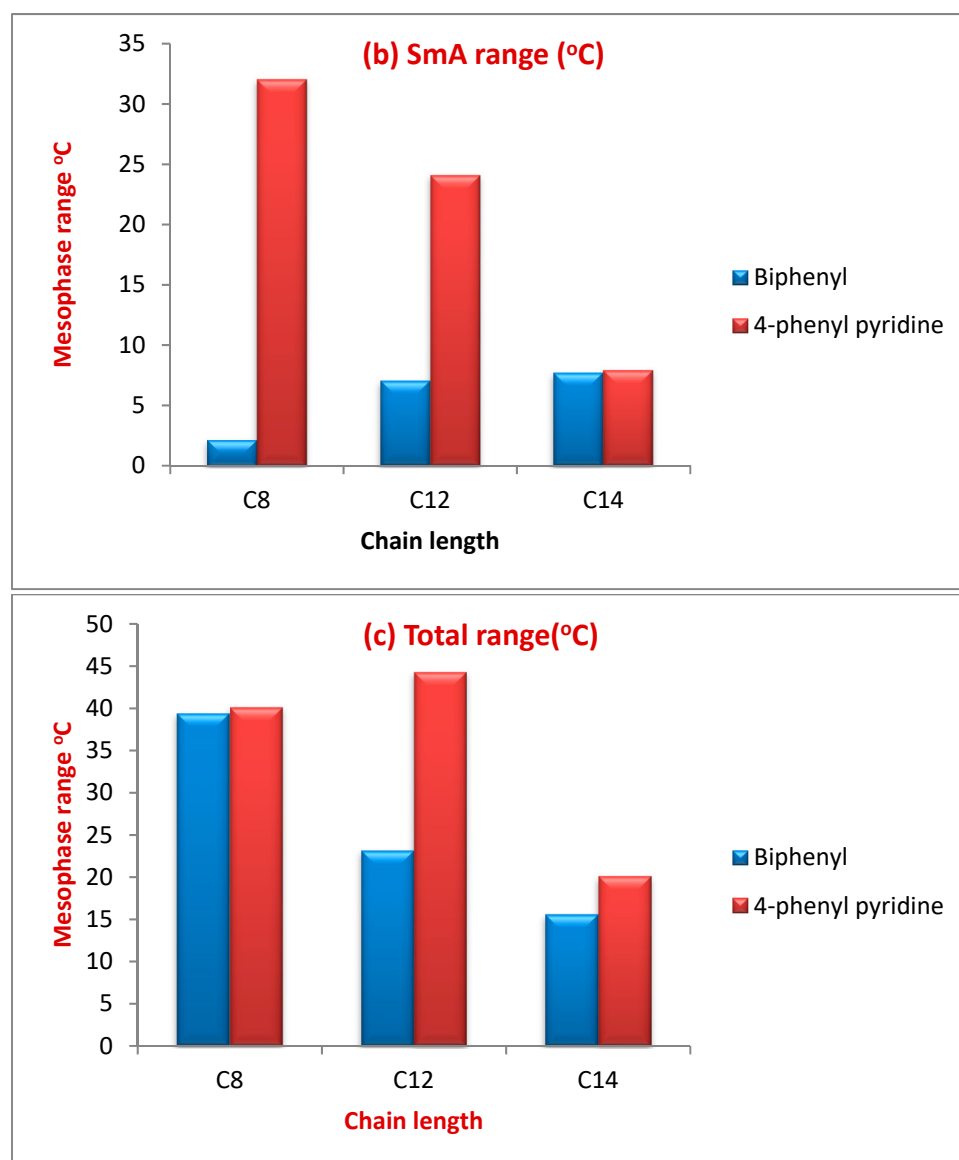


Figure 3. Effect of the alkyl chain length on mesophase behaviour of the biphenyl and 4-phenyl pyridine-based mesogens. (a) Dependence of smectic X1 range on terminal alkyl chain length. (b) Graphical representation of dependence of smectic A range on the terminal chain length. (c) Graphical representation of dependence of total mesomorphic range on the terminal chain length. SmX1 and SmA were identified by the authors in [40] for samples 3.c, 3.d and 3.e (referred to as Biphenyl in this figure) as SmX1 and SmA, respectively.

The variation of mesophase temperature ranges of the different observed textures (SmX1 and SmA) in the new compounds 3.f to 3.g is compared to the results obtained for mesomorphic compounds bearing biphenyl moiety rather than 4-phenyl pyridyl group in their mesogens. The results are displayed in Table 2.

With the exception of the SmX1 temperature range of the C8 compound belonging to the “biphenyl” series, the temperature ranges of both the SmX1 and SmA mesophases of all compounds are higher in compounds 3.f–3.h bearing the 4-phenyl pyridine moiety. In addition, the total mesophase range is generally higher in the 3.f–3.h compounds compared to their biphenyl analogues. The broadening in the mesomorphic temperature range in the compounds 3.f–3.h can be rationalized to the increased pi–pi stacking as a result from the extra contribution of the N atom of the pyridine ring to the total conjugated electrons along the mesogen. This elevation in pi–pi stacking can explain the promoted SmX1 and SmA

mesomorphic order rather than the nematic one even for the sample bearing the shortest alkyl chain length (**3.f**).

Table 2. Variation of mesophase temperature ranges of the different observed textures for the mesomorphic compounds bearing the biphenyl group rather than 4-phenyl pyridine ends in their mesogens. SmX1 and SmA were identified by the authors in [40] for samples **3.c**, **3.d** and **3.e** as SmX1 and SmA, respectively.

Alkyl Chain Length	SmX1 Range (°C)		SmA Range (°C)		Total Range (°C)	
	Biphenyl	4-Phenylpyridine	Biphenyl	4-Phenylpyridine	Biphenyl	4-phenylpyridine
C8	34.9	8.1	2.2	32.0	39.4	40.1
C12	16.1	20.2	7.1	24.1	23.2	44.3
C14	7.9	12.2	7.7	7.9	15.6	20.1

3.3. DFT Calculations

The theoretical DFT calculations were performed in gas phase by Gaussian 9, with the DFT/B3LYP method. Since there was an absence of the imaginary frequency of all optimized structures, they were approved to be stable. The results of the theoretical calculations were the prepared compounds **3.a–3.h**. The results revealed non-planar geometry for all compounds investigated. The phenyl rings were not co-planar and the twist angle of the CH=N was dependent on the degree of conjugation and the arylidene part. Moreover, the biphenyl ring and its pyridyl derivative were very different and this angle deviating from co-planarity was affected by the presence of a heteroatom. The twist angle (θ) of the CH=N varied between 7.0 and 9.4°. The least twist angle was for the pyridyl derivative **3.b** (θ) = 7.0° while its phenyl derivative **3.a** showed **3.b** (θ) = 8.8°, this little difference between them could be illustrated in terms of the aromaticity. The pyridine is known to be less aromatic than its phenyl analogue. A more aromatic phenyl enforces the planarity of the compounds. Similarly, concerning the biphenyl derivative **3.e** and its pyridine analogue **3.h**, the biphenyl showed a twist angle (θ) = 10.0°, while its pyridine derivative showed (θ) = 13.2°. This result could be explained in the terms of better conjugation of the π -cloud of the aromatic rings with the imino group, and consequently a high conjugation led to more enforcement of the conjugated system to make it more planar [41]. While these theoretical molecular geometries may provide a reasonable prediction of the preferred molecular structure in the gas phase, the presence of these compounds in liquid crystalline matter condensed phases which exhibited a different lowest energy and more elongated species were to be preferred [42]. Furthermore, the length of the flexible terminal groups had a broad impact on the mesomorphic manner, either the stability or the structure of the enhanced phase of liquid crystals, and this is often explained in terms of molecular shape [43] (Figure 4).

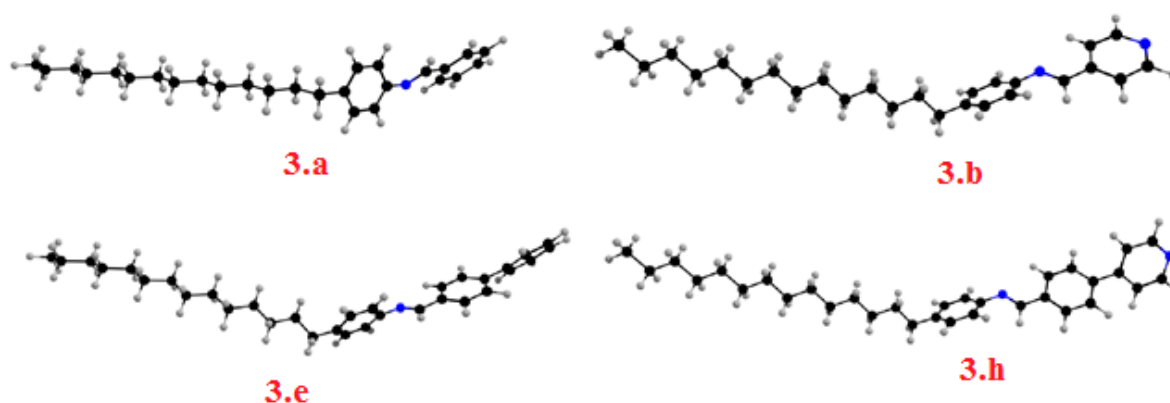


Figure 4. Optimized geometrical structure of the prepared compounds **3.a**, **3.b**, **3.e** and **3.h**.

3.4. Frontier Molecular Orbitals (FMOs)

Table 3 and Figure 5 present the predicted plots of the prepared compounds frontier molecular orbitals HOMO (highest occupied) and LUMO (lowest unoccupied), **3.a**, **3.b**, **3.e** and **3.h**. The electron densities of the sites involved in LUMO formation as well as HOMO formation are localized on the pyridyl part and its conjugated rings, see Figure 5. The degree of the conjugated rings as well as the presence of the hetero atom, on the other hand, had an effect on the electron densities of the FMOs. Moreover, the degree of conjugation and the presence of the N-atom had a significant effect on the FMO energy frontier levels and the frontier molecular orbital energy gap. Levels of the frontier molecular orbitals were impacted by the attachment of more aromatic rings. The presence of the N-atom instead of the carbon significantly lowered the energy level of the frontier molecular orbitals. Moreover, the extraconjugation of the prepared biphenyl derivative **3.b** and its pyridyl derivative **3.f** highly affected the energy difference between the FMOs. However, the pyridyl derivative showed more decrement concerning the energy gap than the phenyl one. This result could be illustrated in terms of increments of the co-planarity in the case of the pyridyl derivative with respect to its phenyl, which resulted in extra conjugation of the aromatic rings and a decrease in the FMO energy gap.

Table 3. FMO Energies e.V. and their values for the prepared compounds **3.a**, **3.b**, **3.e** and **3.h**.

Compounds	HOMO	LUMO	ΔE
3.a	−5.92	−1.75	4.18
3.b	−6.22	−2.18	4.05
3.e	−5.81	−1.92	3.89
3.h	−6.01	−2.14	3.87

3.5. Molecular Electrostatic Potential (MEP)

The charge distribution map for the prepared compounds **3.a**, **3.b**, **3.e** and **3.h** was calculated using the same method on the same basis sets according to molecular electrostatic potential (MEP) as presented in Figure 6. In addition, the molecular electrostatic potential (MEP) is a crucial property for studying the electron density distribution over molecules [44–46]. Furthermore, MEP is one of the most effective methods for determining whether or not a substance has intermolecular and/or intramolecular interactions. Except for the phenyl derivatives **3.a** and **3.e**, the presence of the polar N-atom and the linking CH=N group of the studied compounds had an impact on the localization of the iso-electronic density of the electron rich and electron deficient areas, whereas the CH=N group of the Schiff base part shows the most electron deficient site, while the terminal alkoxy chain is the most electron rich part. The predicted charge distribution maps could be a tool for illustration of the mesophase formation enhanced by the liquid crystals.

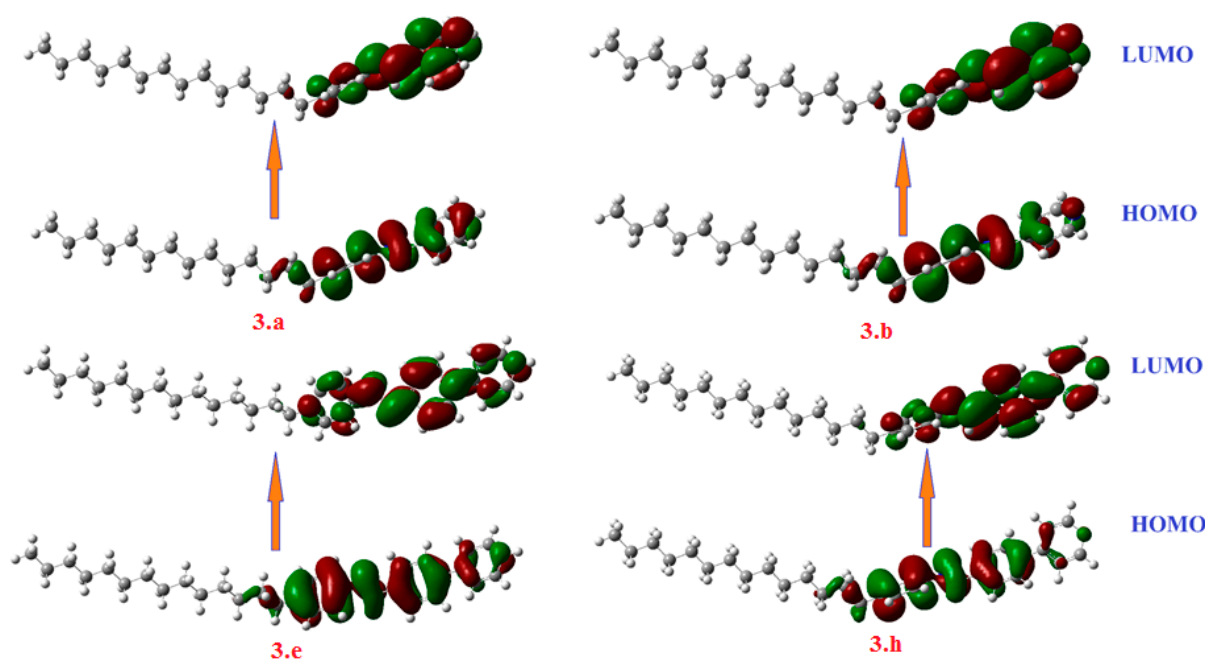


Figure 5. The calculated plots for the prepared compounds 3.a, 3.b, 3.e and h of the frontier molecular orbitals.

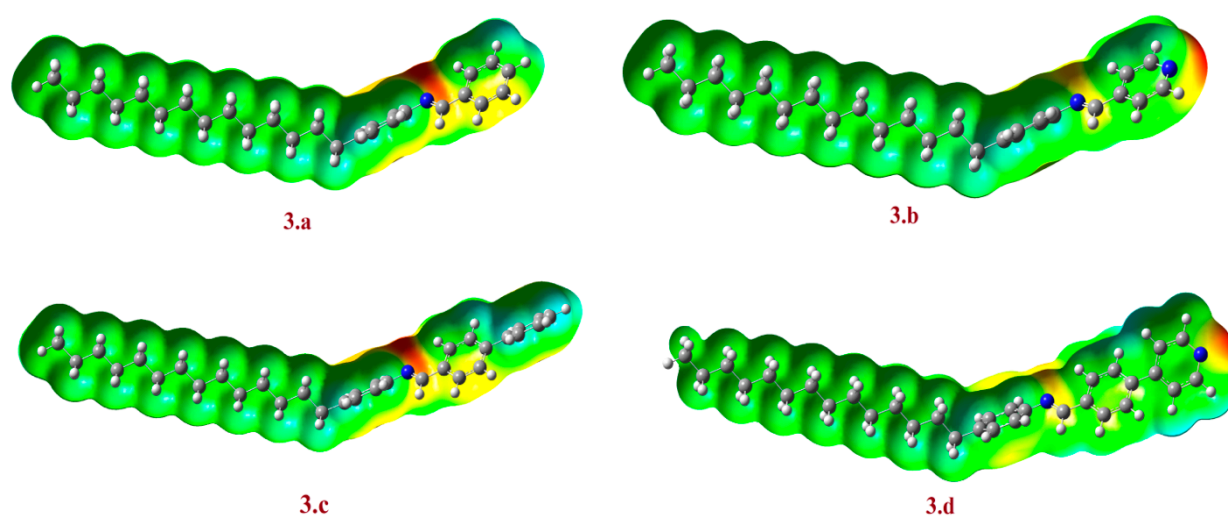


Figure 6. Molecular electrostatic potentials (MEP) for the prepared compounds 3.a, 3.b, 3.e and 3.h.

3.6. Aromaticity, π - π Stacking and LOL- π

Based on optimized geometries of compounds 3.a, 3.b, 3.e and 3.h, the Multiwfn 3.8 code [47] was employed to investigate delocalization, aromaticity and π - π stacking strengths of all phenyl and pyridine rings. Aromaticity and cyclic delocalization were evaluated using the normalized multicenter bond order (MCBO) index, [48] where a larger MCBO value resembles stronger aromatic ring. The π - π stacking strength can be estimated by means of the localized orbital locator integrated π over plane (LOLIPOP) index [49] namely the lesser the LOLIPOP index of a ring, the stronger its π -stacking ability. Moreover, the isosurface of localized orbital locator purely contributed by π -orbitals (LOL- π) [50] was calculated using the Multiwfn code and visualized using the VMD code [51]. The isosurface maps of LOL- π of the studied compounds, as well as calculated LOLIPOP values and normalized MCBO results are displayed in Figure 1. The calculated total number of π orbitals for compounds 3.a, 3.b, 3.e and 3.h are 6, 7, 9 and 10 orbitals, respectively. It can be seen from the occurrence regions and shapes of the LOL- π isosurfaces that C-substitution of

imine with pyridine in compound **3.b** extends conjugation along the N7=C8 bond, besides slightly extending π -conjugation to the first C in the long alkyl chain. Bond length of N7=C8 was found to increase in the order: **3.b** (1.275 Å) < **3.a** = **3.e** (1.276 Å) < **3.h** (1.277 Å), which is in line with the wide range delocalization nature of the localized π -orbitals map of **3.b**. Additionally, strong delocalization of π -electrons can be observed in biphenyl and phenylpyridine moieties. It can also be noticed that all rings have a comparable six-center aromatic conjugation. Quantitative valuation of aromaticity, using normalized MCBO aromaticity index, shows that all inner phenyl rings have the same aromaticity (0.636). Similarly, central phenyl rings of **3.e** and **3.h** have identical aromaticity (0.631). One can also conclude that pyridine and benzene terminal rings of **3.a** and **3.b**, respectively, exhibit a similar degree of cyclic delocalization. From the difference in MCBO values of different rings, terminal benzene and pyridine rings of **3.e** and **3.h** compounds have the strongest aromatic character. When compared to free benzene (**3.a**), central benzene rings of **3.e** and **3.f** suffer a slight but significant reduction of aromaticity. Overall, the most aromatic rings are the terminal ones. According to relative values of the LOLIPOP index, a stronger π -stacking ability is most expected for terminal pyridine rings of **3.b** and **3.f** compounds, while inner phenyl rings of **3.a**, **3.e** and **3.h** are predicted to have the weakest stacking interaction ability. Considering the average LOLIPOP taken over rings located at the molecular periphery, π -stacking strength of studied compounds is predicted to show the trend: **3.b** (6.321) > **3.e** = **3.h** (7.028) > **3.a** (7.202). The results of the aromaticity, π - π stacking and LOL- π could be a good illustration of the mesomorphic behaviour of the investigated compounds, Figure 7.

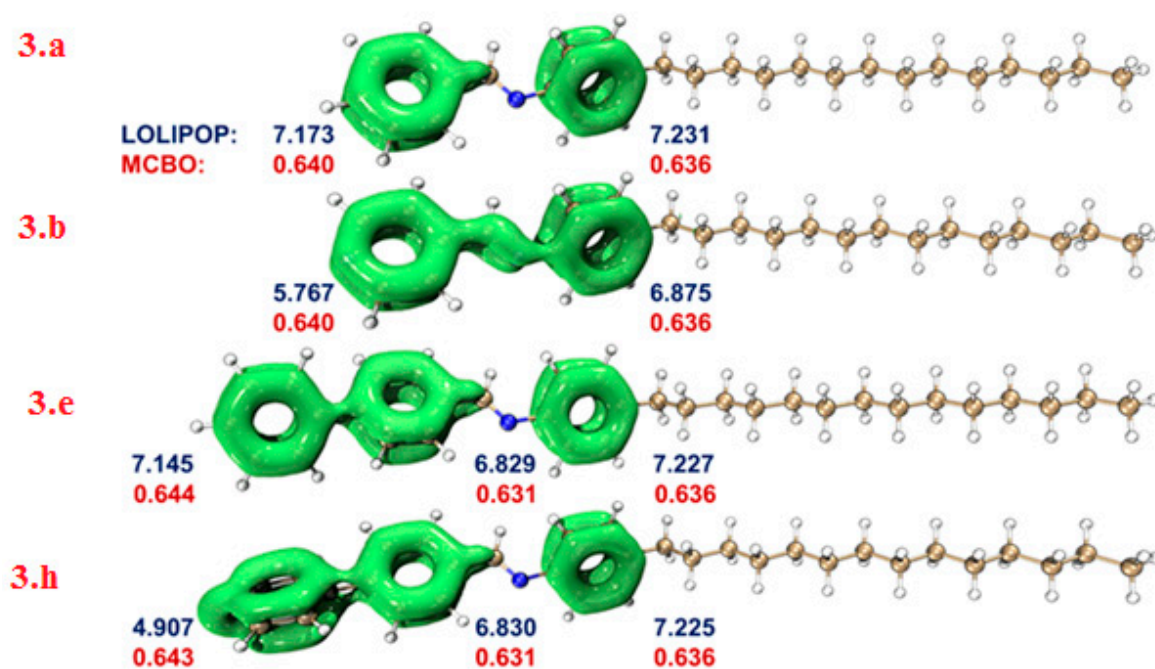


Figure 7. Isosurface maps of LOL- π (Isovalue = 0.3) with labeling for the LOLIPOP index and normalized MCBO aromaticity index.

4. Conclusions

We prepared and investigated novel series of three ring Schiff base liquid crystals made of p-alkyl aniline derivatives and 4-phenyl pyridine-4'-carbaldehyde. Three terminal alkyl substituted anilines were utilized, namely p-octyl, p-dodecyl and p-tetradecyl aniline. The mesomorphic thermal and optical properties of the compounds were defined by DSC and POM. All compounds revealed enantiotropic dimorphic mesophase behaviour; namely, SmX1 and Sm A. Experimental results obtained for these mesophases were correlated with the DFT theoretical calculations. The results of the new series were then compared to

two series of compounds bearing pyridine and biphenyl in their mesogens, respectively. Compounds of one pyridine ring (two aromatic ring Schiff bases) are generally not mesomorphic. The results indicate that the alkyl chain length has significant impact on the mesomorphic characteristics and thermal stabilities of the different mesophases as well. As a trend, the temperature ranges of both the SmX1 and SmA mesophases of all compounds are higher in new compounds bearing the 4-phenyl pyridine moiety. In addition, the overall mesophase range is generally broader in the new compounds when compared to their biphenyl analogues. The increased broadening in the mesomorphic temperature range in the compounds including 4-phenyl pyridine can be explained by an increment in the π - π stacking that emerged by the additional share of the pyridine N atom to the conjugation along the mesogens. This promoted π - π stacking can be interpreted as the preference of smectic mesophase formation rather than the nematic order even for the sample terminated with the shortest alkyl chain length. Finally, the DFT results were carried out to show the non-coplanar geometry for all investigated compounds. The twist angle of the CH=N is found to be dependent on the degree of conjugation and the contributed arylidene part. Moreover, the predicted charge distribution maps could be used as a tool to explain the mesophase preference of the liquid crystals. The results of the estimated aromaticity, π - π stacking and LOL- π were considered to explain the mesomorphic behaviour of the investigated compounds.

Supplementary Materials: The following are available online at <https://www.mdpi.com/article/10.3390/cryst11080978/s1>, Figure S1: ^1H NMR of compound 3.d, Figure S2: ^{13}C NMR of compound 3.d, Figure S3: ^1H NMR of compound 3.e, Figure S4: ^{13}C NMR of compound 3.e, Figure S5: ^1H NMR of compound 3.f, Figure S6: ^{13}C NMR of compound 3.f.

Author Contributions: Data curation, M.A.Z., S.Z.M., K.D.K., M.J. and M.H.; Formal analysis, M.A. and K.D.K.; Funding acquisition, M.A.Z.; Investigation, E.S.H.E.A.; Methodology, M.A. and M.H.; Project administration, S.Z.M. and M.J.; Writing—original draft, K.D.K. and M.H.; Writing—review & editing, Y.E.K. and M.H. All authors have read and agreed to the published version of the manuscript.

Funding: This research was funded by King Saud University, Riyadh, Saudi Arabia. Project number (RSP-2021/402).

Acknowledgments: The authors extend their appreciation to the Researchers Supporting Project number (RSP-2021/402), King Saud University, Riyadh, Saudi Arabia.

Conflicts of Interest: The authors declare no conflict of interest.

References

1. Geelhaar, T.; Griesar, K.; Reckmann, B. 125 years of liquid crystals—A scientific revolution in the home. *Angew. Chem. Int. Ed.* **2013**, *52*, 8798–8809. [[CrossRef](#)]
2. Lin, B.; Chen, S.; Chen, H.; Lee, J.; Wu, S. Liquid crystal display and organic light-emitting diode display: Present status and future perspectives. *Light Sci.* **2018**, *7*, 17168.
3. Bisoyi, H.K.; Li, Q. Light-driven liquid crystalline materials: From photo-induced phase transitions and property modulations to applications. *Chem. Rev.* **2016**, *116*, 15089–15166. [[CrossRef](#)]
4. Han, M.J.; Wei, D.; Kim, Y.H.; Ahn, H.; Shin, T.J.; Clark, N.A.; Walba, D.M.; Yoon, D.K. Highly oriented liquid crystal semiconductor for organic field-effect transistors. *ACS Cent. Sci.* **2018**, *4*, 1495–1502. [[CrossRef](#)]
5. Jiang, M.; Guo, Y.; Yu, H.; Zhou, Z.; Turiv, T.; Lavrentovich, O.D.; Wei, Q.H. Low f-Number Diffraction-Limited Pancharatnam-Berry Microlenses Enabled by Plasmonic Photopatterning of Liquid Crystal Polymers. *Adv. Mater.* **2019**, *31*, 1808028. [[CrossRef](#)]
6. Ula, S.W.; Traugott, N.A.; Volpe, R.H.; Patel, R.R.; Yu, K.; Yakacki, C.M. Liquid crystal elastomers: An introduction and review of emerging technologies. *Liq. Cryst. Rev.* **2018**, *6*, 78–107. [[CrossRef](#)]
7. Jiang, Z.C.; Xiao, Y.Y.; Tong, X.; Zhao, Y. Selective Decrosslinking in Liquid Crystal Polymer Actuators for Optical Reconfiguration of Origami and Light-Fueled Locomotion. *Angew. Chem. Int. Ed.* **2019**, *58*, 5332–5337. [[CrossRef](#)] [[PubMed](#)]
8. Khalid, M.; Shanks, K.; Ghosh, A.; Tahir, A.; Sundaram, S.; Mallick, T.K. Temperature regulation of concentrating photovoltaic window using argon gas and polymer dispersed liquid crystal films. *Renew. Energy* **2021**, *164*, 96–108. [[CrossRef](#)]
9. Zhang, C.; Nakano, K.; Nakamura, M.; Araoka, F.; Tajima, K.; Miyajima, D. Noncentrosymmetric Columnar Liquid Crystals with the Bulk Photovoltaic Effect for Organic Photodetectors. *J. Am. Chem. Soc.* **2020**, *142*, 3326–3330. [[CrossRef](#)]
10. Siddiqi, H.M.; Kun Lin, Y.; Hussain, Z.; Majeed, N. Bovine serum albumin protein-based liquid crystal biosensors for optical detection of toxic heavy metals in water. *Sensors* **2020**, *20*, 298.

11. Lee, M.-J.; Lee, W. Liquid crystal-based capacitive, electro-optical and dielectric biosensors for protein quantitation. *Liq. Cryst.* **2020**, *47*, 1145–1153. [[CrossRef](#)]
12. Wilkinson, T. Applications of liquid crystals in telecommunications. *Handb. Liq. Cryst.* **2014**, *8*, 1–28. [[CrossRef](#)]
13. Yilmaz Canli, N.; Ocak, H.; Okutan, M.; Karanlık, G.; Bilgin Eran, B. Comparative dielectric parameters and conductivity mechanisms of pyridine-based rod-like liquid crystals. *Phase Transit.* **2020**, *93*, 784–792. [[CrossRef](#)]
14. Wang, L.; Hou, Y.; Zhong, X.; Hu, J.; Shi, F.; Mi, H. Preparation and catalytic performance of alginate-based Schiff Base. *Carbohydr. Polym.* **2019**, *208*, 42–49. [[CrossRef](#)] [[PubMed](#)]
15. Baumeister, J.E.; Reinig, K.M.; Barnes, C.L.; Kelley, S.P.; Jurisson, S.S. Technetium and rhenium Schiff base compounds for nuclear medicine: Syntheses of rhenium analogues to ^{99m}Tc-furifosmin. *Inorg. Chem.* **2018**, *57*, 12920–12933. [[CrossRef](#)]
16. Ansari, K.; Chauhan, D.S.; Quraishi, M.; Mazumder, M.A.; Singh, A. Chitosan Schiff base: An environmentally benign biological macromolecule as a new corrosion inhibitor for oil & gas industries. *Int. J. Biol. Macromol.* **2020**, *144*, 305–315. [[PubMed](#)]
17. Guo, S.; Liu, G.; Fan, C.; Pu, S. A new diarylethene-derived probe for colorimetric sensing of Cu (II) and fluorometric sensing of Cu (II) and Zn (II): Photochromism and high selectivity. *Sens. Actuators B Chem.* **2018**, *266*, 603–613. [[CrossRef](#)]
18. Nafee, S.S.; Hagar, M.; Ahmed, H.A.; Alhaddad, O.; El-Shishtawy, R.M.; Raffah, B.M. New two rings Schiff base liquid crystals; ball mill synthesis, mesomorphic, Hammett and DFT studies. *J. Mol. Liq.* **2020**, *299*, 112161. [[CrossRef](#)]
19. Alnoman, R.B.; Hagar, M.; Ahmed, H.A.; Naoum, M.M.; Sobaih, H.A.; Almshaly, J.S.; Haddad, M.M.; Alhaisoni, R.A.; Alsobhi, T.A. Binary liquid crystal mixtures based on schiff base derivatives with oriented lateral substituents. *Crystals* **2020**, *10*, 319. [[CrossRef](#)]
20. Ahmed, H.; Mansour, E.; Hagar, M. Mesomorphic study and DFT simulation of calamitic Schiff base liquid crystals with electronically different terminal groups and their binary mixtures. *Liq. Cryst.* **2020**, *47*, 2292–2304. [[CrossRef](#)]
21. Nakum, K.J.; Katariya, K.D.; Jadeja, R.; Prajapati, A. Schiff base of 4-n-alkoxy-2-hydroxy benzaldehyde with 4-amino acetophenone and their Cu (II) complexes: Synthesis, characterization and mesomorphic behavior. *Mol. Cryst. Liq. Cryst.* **2019**, *690*, 1–13. [[CrossRef](#)]
22. Nakum, K.J.; Katariya, K.D.; Jadeja, R.N. Synthesis, characterization, and mesomorphic properties of some new Schiff base homologues series and their Cu (II) complexes. *Mol. Cryst. Liq. Cryst.* **2020**, *708*, 1–13. [[CrossRef](#)]
23. Cîrcu, V.; Mocanu, A.S.; Roşu, C.; Manaila-Maximean, D.; Dumitraşcu, F. Thermal behaviour and electro-optical properties of a series of liquid crystals based on palladium complexes with mixed ligands: Schiff bases and N-benzoyl thioureas. *J. Therm. Anal. Calorim.* **2012**, *107*, 877–886. [[CrossRef](#)]
24. Roşu, C.; Manaila-Maximean, D.; Cîrcu, V.; Molard, Y.; Roisnel, T. Differential negative resistance in the current–voltage characteristics of a new palladium (II) metallomesogen. *Liq. Cryst.* **2011**, *38*, 757–765. [[CrossRef](#)]
25. Patel, R.V.; Panchal, J.G.; Rana, V.; Menon, S.K. Liquid crystals based on calix [4] arene Schiff bases. *J. Incl. Phenom. Macrocycl. Chem.* **2010**, *66*, 285–295. [[CrossRef](#)]
26. Vardar, D.; Ocak, H.; Akdaş Kılıç, H.; Jeannin, O.; Camerel, F.; Eran, B.B. Synthesis and characterization of new pyridine-based chiral calamitic liquid crystals. *Liq. Cryst.* **2020**, 850–861. [[CrossRef](#)]
27. Nafee, S.S.; Ahmed, H.; Hagar, M. Theoretical, experimental and optical study of new thiophene-based liquid crystals and their positional isomers. *Liq. Cryst.* **2020**, *47*, 1291–1302. [[CrossRef](#)]
28. Chakraborty, I.; Bodurtha, K.J.; Heeder, N.J.; Godfrin, M.P.; Tripathi, A.; Hurt, R.H.; Shukla, A.; Bose, A. Massive electrical conductivity enhancement of multilayer graphene/polystyrene composites using a nonconductive filler. *ACS Appl. Mater. Interfaces* **2014**, *6*, 16472–16475. [[CrossRef](#)]
29. Fouad, F.S.; Ness, T.; Wang, K.; Ruth, C.E.; Britton, S.; Twieg, R.J. Biphenyl-1, 2, 4-oxadiazole based liquid crystals—synthesis, mesomorphism, effect of lateral monofluorination. *Liq. Cryst.* **2019**, *46*, 2281–2290. [[CrossRef](#)]
30. Ibraheem, T.K.; Karam, N.H.; Al-Dujaili, A.H. Synthesis and characterization of symmetrical liquid crystalline compounds based on oxazole and thiazole rings. *Mol. Cryst. Liq. Cryst.* **2020**, *710*, 1–12. [[CrossRef](#)]
31. Devadiga, D.; Ahipa, T. Heterodimeric hydrogen-bonded mesogens comprising pyridine moiety: A review. *Liq. Cryst. Rev.* **2020**, *8*, 5–28. [[CrossRef](#)]
32. Hagar, M.; Ahmed, H.; Saad, G. New calamitic thermotropic liquid crystals of 2-hydroxypyridine ester mesogenic core: Mesophase behaviour and DFT calculations. *Liq. Cryst.* **2020**, *47*, 114–124. [[CrossRef](#)]
33. Vardar, D.; Akdaş Kılıç, H.; Ocak, H.; Jeannin, O.; Camerel, F.; Eran, B.B. Pyridine-based chiral smectogens: Effects of polar end groups on liquid crystal properties. *Liq. Cryst.* **2020**, 1–10. [[CrossRef](#)]
34. Petrov, V.F. Nitrogen-containing fused heterocycles as the structural fragments in calamitic liquid crystals. *Liq. Cryst.* **2001**, *28*, 217–240. [[CrossRef](#)]
35. Nash, J.; Gray, G. Studies of some heterocyclic mesogens. *Mol. Cryst. Liq. Cryst.* **1974**, *25*, 299–321. [[CrossRef](#)]
36. Liu, C.Y.; Huang, C.H.; Cheng, P.S.; Tsai, W.L. Aromatic heterocycles used as terminal groups of calamitic liquid crystals. *J. Chin. Chem. Soc.* **2012**, *59*, 81–86. [[CrossRef](#)]
37. Ong, L.-K.; Ha, S.-T.; Yeap, G.-Y.; Lin, H.-C. Heterocyclic pyridine-based liquid crystals: Synthesis and mesomorphic properties. *Liq. Cryst.* **2018**, *45*, 1574–1584. [[CrossRef](#)]
38. Muniprasad, M.; Srinivasulu, M.; Chalapathi, P.; Potukuchi, D. Induction of liquid crystalline phases and influence of chain length of fatty acids in linear hydrogen-bonded liquid crystal complexes. *Mol. Cryst. Liq. Cryst.* **2012**, *557*, 102–117. [[CrossRef](#)]

39. Srinivasu, C.; Pisipati, V.G.; Prabhu, C.R.; Murty, P.N.; Lakshminarayana, S. Phase transitions in p-(phenyl benzylidene)-p1-alkylaniline compounds: A dilatometric study. *Z. Für Nat. A* **2007**, *62*, 75–83. [[CrossRef](#)]
40. Bhagavath, P.; Mahabaleshwara, S.; Bhat, S.G.; Potukuchi, D.; Shetty, P.; Maddasani, S. Influence of polar substituents and flexible chain length on mesomorphism in non-mesogenic linear hydrogen bonded complexes. *J. Mol. Liq.* **2021**, *336*, 116313. [[CrossRef](#)]
41. Hagar, M.; Ahmed, H.; Alhaddad, O. Experimental and theoretical approaches of molecular geometry and mesophase behaviour relationship of laterally substituted azopyridines. *Liq. Cryst.* **2019**, *46*, 1440–1451. [[CrossRef](#)]
42. Paterson, D.A.; Abberley, J.P.; Harrison, W.T.; Storey, J.M.; Imrie, C.T. Cyanobiphenyl-based liquid crystal dimers and the twist-bend nematic phase. *Liq. Cryst.* **2017**, *44*, 127–146. [[CrossRef](#)]
43. Hagar, M.; Ahmed, H.; El-Sayed, T.; Alnoman, R. Mesophase behavior and DFT conformational analysis of new symmetrical diester chalcone liquid crystals. *J. Mol. Liq.* **2019**, *285*, 96–105. [[CrossRef](#)]
44. Scrocco, E.; Tomasi, J. Electronic molecular structure, reactivity and intermolecular forces: An heuristic interpretation by means of electrostatic molecular potentials. In *Advances in quantum chemistry*; Elsevier: Amsterdam, The Netherlands, 1978; Volume 11, pp. 115–193.
45. Politzer, P.; Murray, J.S. Relationships between dissociation energies and electrostatic potentials of C-NO₂ bonds: Applications to impact sensitivities. *J. Mol. Struct.* **1996**, *376*, 419–424. [[CrossRef](#)]
46. Marks, T.J.; Ratner, M.A. Design, synthesis, and properties of molecule-based assemblies with large second-order optical nonlinearities. *Angew. Chem. Int. Ed. Engl.* **1995**, *34*, 155–173. [[CrossRef](#)]
47. Lu, T.; Chen, F. Multiwfn: A multifunctional wavefunction analyzer. *J. Comput Chem.* **2012**, *33*, 580–592. [[CrossRef](#)]
48. Giambiagi, M.; de Giambiagi, M.S.; Mundim, K.C. Definition of a multicenter bond index. *Struct. Chem.* **1990**, *1*, 423–427. [[CrossRef](#)]
49. Gonthier, J.F.; Steinmann, S.N.; Roch, L.; Ruggi, A.; Luisier, N.; Severin, K.; Corminboeuf, C. π -Depletion as a criterion to predict π -stacking ability. *Chem. Commun.* **2012**, *48*, 9239–9241. [[CrossRef](#)]
50. Lu, T.; Chen, Q. A simple method of identifying π orbitals for non-planar systems and a protocol of studying π electronic structure. *Theor. Chem. Acc.* **2020**, *139*, 1–12. [[CrossRef](#)]
51. Humphrey, W.; Dalke, A.; Schulten, K. VMD: Visual molecular dynamics. *J. Mol. Graph.* **1996**, *14*, 33–38. [[CrossRef](#)]